Proceedings of the 1st international Symposium on AI and Fluid Mechanics
Paper No S5 P7

Enhanced LES Predictions Through Multi-Fidelity Integration Using High-Fidelity Point Selection Strategy

Thomas Berthelon*[1], Ali Mahdi[1], and Guillaume Balarac[1]

[1]Université Grenoble Alpes, CNRS, Grenoble-INP, LEGI, Grenoble, France

Keywords: Turbulent flows, Large Eddy Simulation, Multi-fidelity, Adaptive Sampling Strategy

Abstract. Reynolds-Averaged Navier-Stokes (RANS) methods offer the most affordable computational cost, but often lack accuracy in capturing complex behaviors. Large Eddy Simulation (LES) provides higher accuracy but is computationally expensive, limiting its use for large parameter spaces. To overcome these limitations, multi-fidelity methods appear as a promising strategy, by combining accurate but sparse results from high-fidelity methods with more approximate but numerous results from low- fidelity methods. However, the application of multi-fidelity strategies within the RANS-LES framework remains underexplored in the literature. In this work, we use a multi-fidelity strategy based on Artificial Neural Networks (ANN) to improve the prediction of turbulent flows. We also introduce an adaptive sampling strategy to select high-fidelity LES points for efficient allocation of computational resources. The proposed strategy was first validated on an analytical test case, before being applied to turbulent flow around an airfoil. Our results show that, despite the limitations of RANS methods, valuable information can be extracted from them to improve the efficiency and effectiveness of LES.

1. Introduction

Computational Fluid Dynamics (CFD) simulations are essential as an engineering tool, especially for conducting parametric studies or evaluating machine performance across various operating conditions. For example, they are used to determine the efficiency of a turbine based on the flow rate passing through it. To date, the Reynolds Averaged Navier-Stokes (RANS) approach is widely used in design offices because of its low calculation cost. However, the simplifying assumptions on which this approach is based can limit the accuracy of predictions. Because of these limitations, RANS methods are generally considered to be low-fidelity approaches. To overcome these shortcomings, an alternative method, Large Eddy Simulation (LES), is beginning to be adopted by industry. This method makes it possible to explicitly solve large scale structures while modeling the smallest scales, which significantly improves the accuracy of predictions compared with RANS methods. However, the computational cost associated with LES remains prohibitive for design purposes. Due to its high cost, the LES method can only be used to study a limited number of operating points.

Multi-fidelity methods involve combining accurate but sparse results from high-fidelity methods (such as LES) with more approximate but numerous results from low-fidelity methods (such as RANS). This approach makes it possible to cover a larger parameter space while maintaining a certain level of overall accuracy. The first research on these methods dates back to the work of Kennedy and O'Hagan in 2000 [9], and they have since been applied in various fields. For a full review of the different multi-fidelity methods, see Fernandez [4]. Most multi-fidelity models are traditionally built using Gaussian Processes (GP) [5, 11] due to their ability to quantify uncertainty and provide reliable estimates. Despite their effectiveness, new developments in multi-fidelity modeling have incorporated Artificial Neural Networks (ANN) as an alternative to GP-based methods. These ANN-based approaches have demonstrated strong performance in handling complex functions that involve non-linearities, phase shifts, and discontinuities [13].

*thomas.berthelon@univ-grenoble-alpes.fr

In fluid mechanics, multi-fidelity models were initially based on GP. Several studies have applied these methods to Euler and RANS approaches [6, 8]. Multi-fidelity models combining RANS and LES approaches remain scarce. To the best of our knowledge, the work of Mole et al. [14] is the only study to explore such a combination within a multi-fidelity framework. Moreover, they did not address the selection of high-fidelity sampling locations, as the high-fidelity points were uniformly distributed.
In this work, we aim to demonstrate the potential of multi-fidelity methods within the RANS-LES framework, a context that remains underexplored in the literature. This framework can involve cases with discontinuities, necessitating the use of neural networks to effectively capture complex relationships between fidelity levels. To address these challenges, we propose a simple high-fidelity point selection strategy that is independent of the specific multi-fidelity method employed. In this work, the strategy is applied to classical ANN-based multi-fidelity methods, providing an effective and practical solution for selecting high-fidelity points and improving the overall description of the target function. First, the procedure to select high-fidelity point is detailed. Then, this procedure is evaluated on an analytic case, characterized by a discontinuity and a phase shift between high and low fidelity data. The procedure is compared to GP-based approach in particular. And finally, the procedure is used in a context that combines the RANS and LES results of a NACA0012 airfoil.

2. High-Fidelity Point Selection Strategy

2.1.Multi-fidelity framework

The multi-fidelity method is first briefly reminded. The method used in this work is similar to the method used by Mole et al. [14], which is akin to that proposed by Meng and Karniadakis [13]. The focus is on analyzing the evolution of a quantity of interest, y, as a function of the input parameter x. To account for varying levels of model precision, two fidelity levels are introduced: $y_H(x)$, representing the high-fidelity function, which offers greater accuracy at the expense of higher computational cost, and $y_L(x)$, the low-fidelity function, which has a lower computational cost but less precision. Multi-fidelity approaches aim to establish a relationship not only between y_H and x, but also between y_H and y_L. The goal is to determine the potentially non-linear function f that links y_H to both x and y_L, expressed as

$$y_H = f(x, y_L). \tag{1}$$

The procedure used to determine f involves training two neural networks. First, the low-fidelity network is trained to be able to evaluate y_L for all x. Training involves n_L low-fidelity evaluations, i.e. $y_{L,i}(x_{L,i})$ with $i = 0...n_L$. Next, this network is used to predict the low-fidelity results for the high-fidelity parameters, i.e. $y_L(x_{H_i})$ with $i = 0..n_H$ and where n_H corresponds to the number of high-fidelity evaluations. Finally, the second network is trained with input $(x_{H_i},\, y_L(x_{H_i}))$. For both networks, the Mean Squared Error (MSE) cost function is minimized using the L-BFGS algorithm [3].
In order to choose certain parameters that are difficult to intuit, a hyperparameter tuning phase is carried out. Given the small amount of data in the cases evaluated, the Leave One Out Cross Validation (LOOCV) method is used. Hyperparameter tuning is used to select the activation functions (hyperbolic tangent or logistic function) and the intensity of the regularization. In order to take into account a possible phase shift between the two fidelity levels, a hyperparameter τ is added,

$$y_H = f\big(x,\, y_L(x-\tau)\big). \tag{2}$$

The user chooses different values of τ, in practice equidistant between a minimum value and a maximum value of phase shift. Each value is evaluated using the LOOCV method. Finally, the value with the lowest MSE is chosen to make the prediction. Note that this method assumes that there is a single phase shift between the two fidelity levels. In order to take into account more complex phase shift relationships, it is possible to use embedding theory [13].

2.2.Description of the strategy

An automated strategy for selecting high-fidelity points is introduced to minimize computational costs by efficiently choosing evaluation points. While GP-based methods provide uncertainty quantification, which enables point selection strategies, to our knowledge, no equivalent approach has been proposed for ANN-based methods. An effective and practical solution is then provided in this work for selecting high-fidelity points. First, the user defines the parameter range $[x_{\min}, x_{\max}]$, and the low-fidelity function is densely evaluated within this range. Since low-fidelity evaluations are computationally cheap, this step does not require significant optimization. In order

to perform the first multi-fidelity estimation, we add a third high-fidelity point. We choose it based on the maximum of the Hessian of the low-fidelity function. Once the third point is added, the initial multi-fidelity prediction $y_{MF}(x)$ is computed. Then it is compared to a piecewise linear prediction y_{lin} based on the high-fidelity points, where the latter is defined as:

$$y_{lin}(x) = y_i + \frac{y_{i+1} - y_i}{x_{i+1} - x_i} \cdot (x - x_i), \quad \text{for } x_i \leq x \leq x_{i+1}. \tag{3}$$

The multi-fidelity and linear predictions are compared in order to compute an *interpolation error*:

$$\tilde{\epsilon}(x) = |y_{MF}(x) - y_{lin}(x)| \,. \tag{4}$$

The next point x_H is then chosen where this interpolation error is maximum,

$$x_H = \arg\max_x \tilde{\epsilon}(x). \tag{5}$$

This operation is repeated until the L_2-norm of the interpolation error reaches a user-defined threshold.

3.Validation on Analytical Case

The proposed procedure is first tested on an analytical test case, based on the "Forrester" function with a jump [18], to which a phase shift $\tau = 0.1$ has been added. The functions y_H and y_L are defined by:

$$y_L(x) = \begin{cases} 0.5(6x-2)^2 \sin(12x-4) + 10(x-0.5) - 5, & x \leq 0.5, \\ 3 + 0.5(6x-2)^2 \sin(12x-4) + 10(x-0.5) - 5, & x > 0.5, \end{cases} \tag{6}$$

$$y_H(x) = \begin{cases} 2\, y_L(x-\tau) - 20(x-\tau) + 20, & x - \tau \leq 0.5, \\ 4 + 2\, y_L(x-\tau) - 20(x-\tau) + 20, & x - \tau > 0.5. \end{cases} \tag{7}$$

The low-fidelity function is evaluated on 26 points, with a high density near the discontinuity. For the multi-fidelity prediction, we use a neural network with two layers of 30 neurons throughout the procedure. Training is performed for 11 values of τ (from 0 to 0.2) evaluated using LOOCV.

Figure 1 illustrates the first six iterations of the procedure. For each iteration, the true high-fidelity function, the true low-fidelity function, the multi-fidelity prediction, and the piecewise linear prediction are displayed. The interpolation error $\tilde{\epsilon}$ from Eq. (4) is also shown, and the next point is identified by a vertical line.

Initially, Figure 1a shows that the third point is $x_H = 0.5$, and the phase shift is overestimated. In iteration 2 (Figure 1b), the next point is $x_H = 0.71$, where $\tilde{\epsilon}$ is the maximum. Iterations continue, adding points near the discontinuity and refining the capture of the phase shift. By iteration 6 (Figure 1f), we see a higher density of points near the discontinuity, which is precisely the expected behavior.

To quantify the error in this analytic case, we define $\epsilon = y_{MF} - y_H$. Figure 2 presents the L_2-norm and L_∞-norm of this error as a function of the number of high-fidelity points. We compare the proposed strategy to two alternative approaches: a classical Gaussian Process (GP)-based multi-fidelity method, where the next point is selected at the location of maximum GP uncertainty (commonly used in Bayesian optimization), and an ANN-based multi-fidelity model with uniformly distributed high-fidelity points.

As shown in Figure 2, our method achieves significantly lower errors, especially for the L_∞-norm after five high-fidelity points. The GP-based strategy struggles with the discontinuity, as shown in Figure 3a, leading to large errors near the discontinuity. Meanwhile, uniform sampling with an ANN (Figure 3b) captures the discontinuity but fails to resolve the phase shift precisely, resulting in a higher L_∞ error.

This analysis highlights the effectiveness of our proposed selection strategy for signals exhibiting both a discontinuity and a phase shift between fidelity levels.

4.Application on Turbulent Flow

4.1.Numerical method

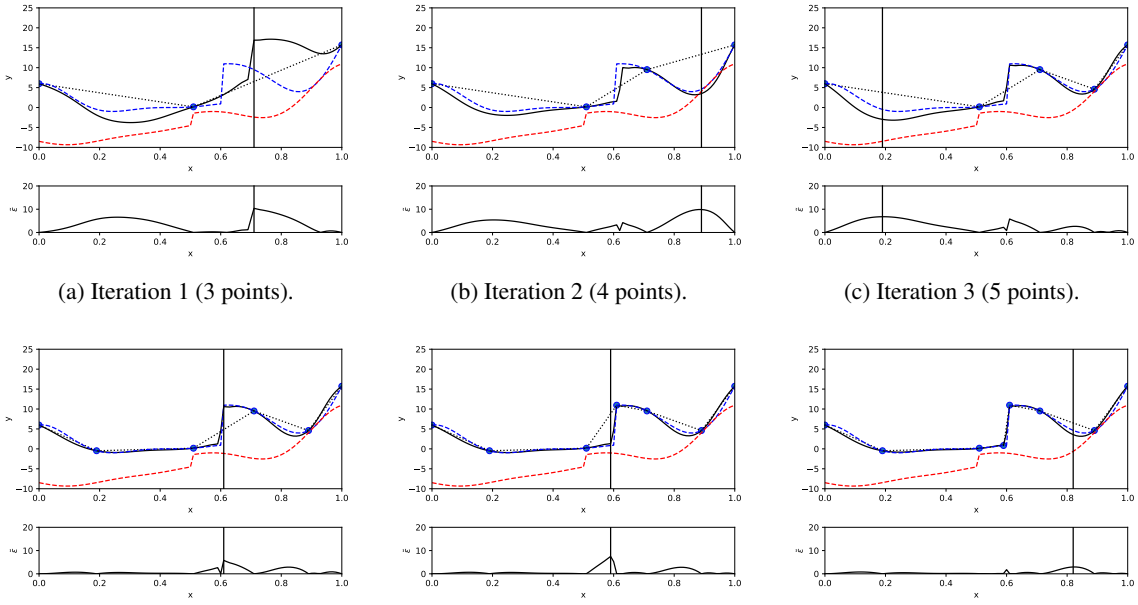

(a) Iteration 1 (3 points). (b) Iteration 2 (4 points). (c) Iteration 3 (5 points).

(d) Iteration 4 (6 points). (e) Iteration 5 (7 points). (f) Iteration 6 (8 points).

Figure 1: Iterations of the procedure applied to the discontinuity-shifted test case, Eq. (6) and (7). At the top of each subfigure: *Dashed red* line—true low-fidelity function; *Dashed blue* line—true high-fidelity function; *Blue* symbols—high-fidelity data; *Dotted black* line—piece-wise linear interpolation; *Black* line—multi-fidelity prediction. At the bottom: interpolation error function.

Simulations use the YALES2 incompressible fractional-step solver [15] with a finite-volume formulation and high-order space-centered schemes dealing with unstructured meshes composed of tetrahedral elements. LES employs a fourth-order Runge-Kutta time advancement [10], while RANS uses an implicit linearized integration [2]. The Spalart-Allmaras model [19] is used for RANS, and the σ-model [16] for LES. We simulate a NACA0012 airfoil at varying angles of attack α for a Reynolds number $Re = \frac{Uc}{\nu} = 50,000$, where c is the chord length, U the inlet velocity, and ν the kinematic viscosity. The geometry is meshed with automatically mesh adaptation strategy [1, 7]. RANS uses a 2D domain of $25c \times 20c$, while LES uses a 3D domain of $30c \times 30c \times c$. A constant and homogeneous velocity U with an angle of attack of α is imposed as inlet condition, whereas a convective outflow boundary condition is used as outlet. Periodic conditions are used on others boundaries.
Figure 4 compares the flow for two angles of attack, $8°$ and $16°$. LES reveals 3D turbulent structures (top and middle rows). The RANS results (bottom row) capture the mean flow topology, showing attached flow at $8°$ and a large recirculation region (stall) at $16°$. In this configuration, the CPU cost of LES is about 10,000 times that of RANS (due to 2D RANS meshes and the significant temporal averaging required in LES).

4.2.Multi-fidelity strategy based on RANS and LES data

We apply our procedure to a realistic case where the low fidelity corresponds to the RANS and the high fidelity corresponds to the LES. A phase-shift parameter τ from -4 to +4 degrees is tested via LOOCV, and the network has 3 layers with 12 neurons. Figure 5 shows the first three iterations. By iteration 3, with only five high-fidelity points, the interpolation error is low, capturing the overall shape, including stall. Figure 6 compares the final multi-fidelity prediction (black line) with LES data not used in training (orange symbols), showing strong agreement and validating the approach. Although RANS is less accurate in highly separated flows, it provides useful information to efficiently guide LES evaluations. Note that, the final multi-fidelity prediction may not pass through all high-fidelity points due to network size and LES statistical uncertainties. Future work could integrate uncertainty estimation [17] and adapt the neural network architecture during point selection.

5.Conclusion

This work introduced an efficient approach for predicting a quantity of interest in turbulent flow simulations. By

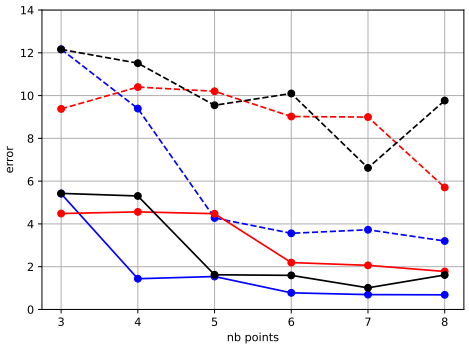

Figure 2: Comparison of error convergence (L_2- and L_∞-norms) for the discontinuity-shifted test case, Eqs. (6) and (7). *Blue*: Proposed ANN strategy, *red*: GP-based strategy (classic), *black*: Uniformly distributed points (ANN).

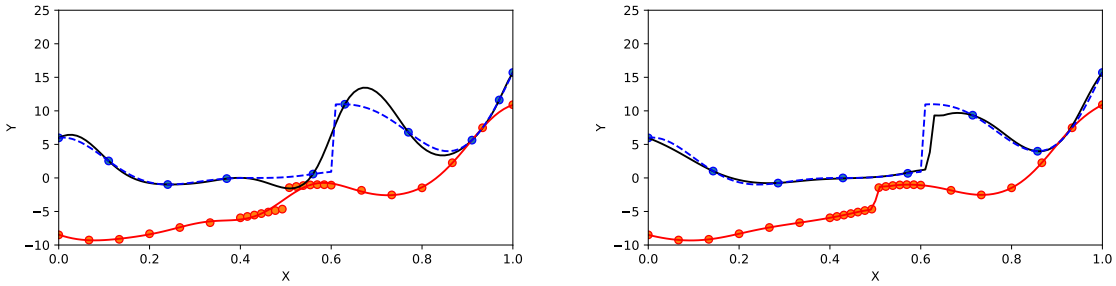

(a) GP-based strategy (8 points).

(b) Uniform points with ANN (8 points).

Figure 3: Multi-fidelity prediction using alternative strategies with 8 points on the discontinuity-shifted test case. *Red* dots = low-fidelity data, *red* line = low-fidelity function, *blue* dots = high-fidelity data, *dashed blue* line = high-fidelity function, *black* line = multi-fidelity prediction.

combining an ANN-based multi-fidelity method (sparse LES with abundant RANS data) and an automated high-fidelity point selection strategy, we minimized costly LES evaluations. The selection strategy was first validated on an analytic case with a discontinuity and phase shift, outperforming standard GP-based and uniform sampling approaches. Finally, in a realistic scenario combining RANS and LES for a NACA0012 airfoil, the method rapidly identified the stall zone and achieved accurate predictions with minimal LES evaluations. These results demonstrate the potential of multi-fidelity methods for CFD, particularly for capturing complex phenomena like stall. Future work includes integrating Bayesian uncertainty estimation, dynamically adapting the network architecture, and extending to higher-dimensional parameter spaces.

Funding Information: The authors gratefully acknowledge support from NETHUNS project under grant ANR-21-CHIN-0001-01.

Acknowledgements: This work was granted access to the HPC resources of CINES/TGCC/IDRIS under the project 2A00611 made by GENCI. Part of this work has been initiated during the Extreme CFD Workshop & Hackathon (`https://ecfd.coria-cfd.fr`).

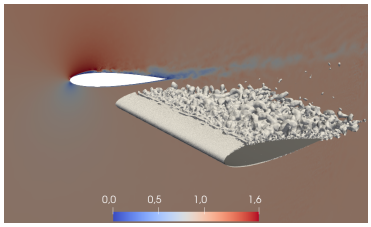

(a) Q-criterion, $\alpha = 8^\circ$ (LES).

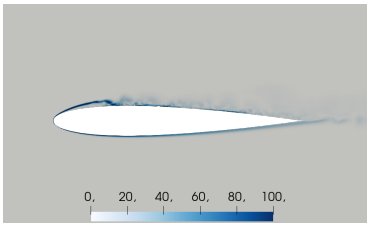

(b) Vorticity magnitude, $\alpha = 8^\circ$ (LES).

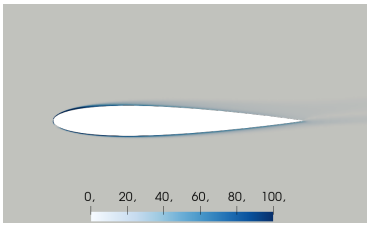

(c) Mean vorticity magnitude, $\alpha = 8^\circ$ (RANS).

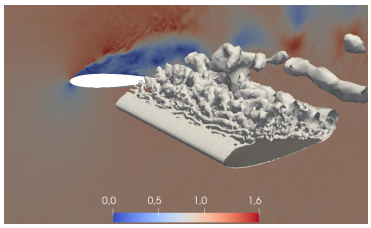

(d) Q-criterion, $\alpha = 16^\circ$ (LES).

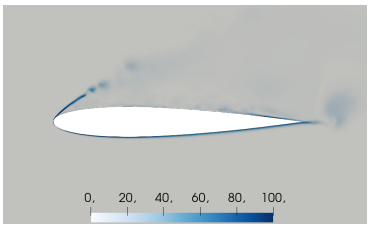

(e) Vorticity magnitude, $\alpha = 16^\circ$ (LES).

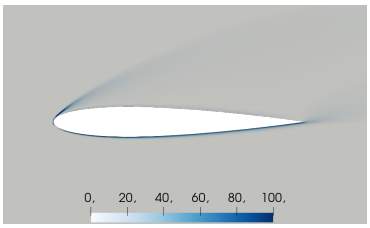

(f) Mean vorticity magnitude, $\alpha = 16^\circ$ (RANS).

Figure 4: Turbulent flow around a NACA0012 airfoil at angles of attack $\alpha = 8^\circ$ (*top row*) and $\alpha = 16^\circ$ (*bottom row*). Left: Q-criterion with instantaneous velocity magnitude (LES), center: instantaneous vorticity magnitude (LES), right: mean vorticity magnitude (RANS).

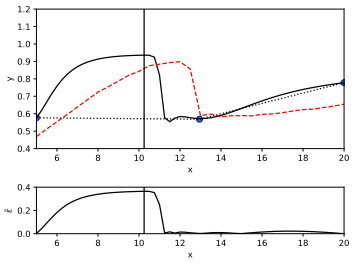

(a) Iteration 1 (3 pts).

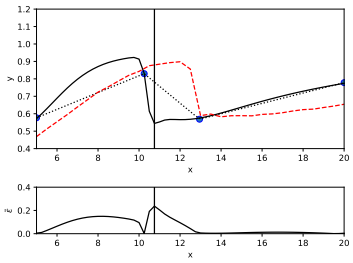

(b) Iteration 2 (4 pts).

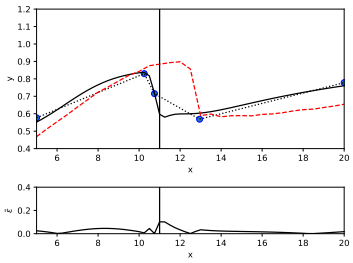

(c) Iteration 3 (5 pts).

Figure 5: First three iterations of the procedure for RANS (low fidelity) + LES (high fidelity). Top: *dashed red* line = RANS interpolation, *blue* symbols = LES data used in training, *dotted black* line = piecewise linear interpolation, *black* line = multi-fidelity prediction. Bottom: Interpolation error $\tilde{\epsilon}$.

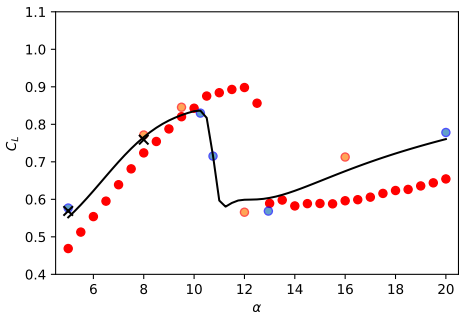

Figure 6: Lift coefficient vs. angle of attack. *Red symbols*: RANS (low fidelity), *black* line: Multi-fidelity prediction, *blue symbols*: LES data used for training, *orange symbols*: Additional LES validation points, *black crosses*: DNS data [12].

Appendix A

RANS with various Reynolds number values:

As an intermediate step, we create an emulated multi-fidelity scenario using two Reynolds numbers in RANS: $Re = 50{,}000$ for low fidelity and $Re = 100{,}000$ for high fidelity. Because RANS is relatively affordable, we can evaluate the lift coefficient C_L for both fidelities on $n_\alpha = 30$ angles of attack, from $5°$ to $20°$. This allows a direct measure of the high-fidelity curve and an error analysis:

$$|\epsilon|_2 = \sqrt{\frac{1}{n_\alpha}\sum_{i}^{n_\alpha}(y_{MF,i} - y_i)^2}, \quad |\epsilon|_\infty = \max_i |y_{MF,i} - y_i|. \tag{8}$$

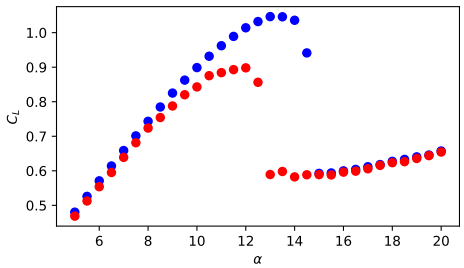

Figure 7: Lift coefficient versus angle of attack for two RANS Reynolds numbers: *red* line = $Re = 50{,}000$ (low fidelity), *blue* line = $Re = 100{,}000$ (high fidelity).

Figure 7 shows the lift coefficient curves for these two Reynolds numbers. Both exhibit a linear region at low α, a sharp drop (stall) at higher α, and a nearly constant C_L beyond stall. The difference in Reynolds number shifts the stall angle and maximum C_L. Figure 8 shows the first six iterations of the high-fidelity point selection strategy, ensuring rapid convergence of the multi-fidelity prediction. Figure 9 compares the error evolution versus the number of high-fidelity points for three approaches: the proposed strategy (ANN + adaptive points), the GP-based strategy (selection via GP uncertainty), and the naive strategy (ANN + uniform point distribution).
For a small number of points, the three methods give comparable errors. However, beyond six points, the L_∞-norm drops dramatically for the proposed method, whereas it remains relatively high for the others. In particular, GP-based selection fails to refine near the stall discontinuity, leading to a plateau in error. A brief sensitivity study on the neural network size is performed (Figure 10), using three architectures: $(10, 10, 10)$, $(20, 20, 20)$, and $(20, 20, 20, 20)$. Although slight disparities occur with fewer points, all converge to the same error level. Thus, the procedure is robust to network size, but an automatic method to adapt the network size during the process is a natural next step.

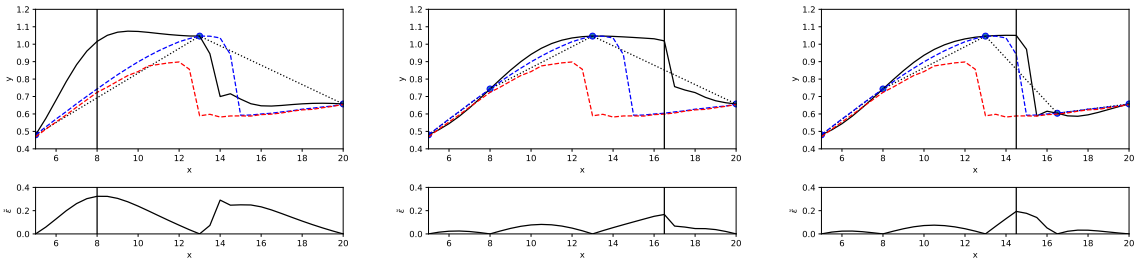

(a) Iteration 1 (3 pts). (b) Iteration 2 (4 pts). (c) Iteration 3 (5 pts).

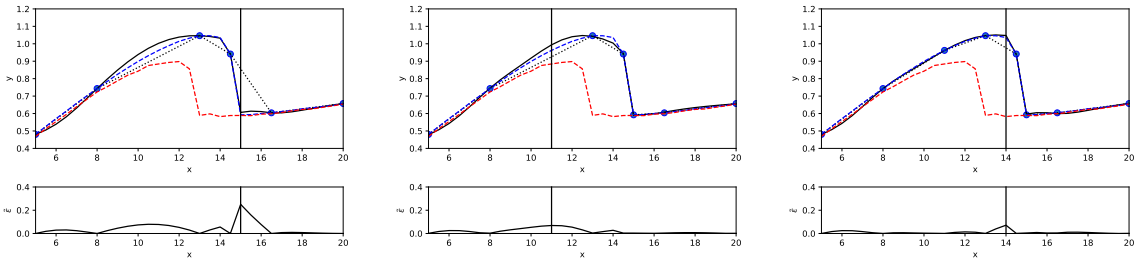

(d) Iteration 4 (6 pts). (e) Iteration 5 (7 pts). (f) Iteration 6 (8 pts).

Figure 8: First six iterations of the automated procedure for RANS at two Reynolds numbers. Top: *dashed red* line = low-fidelity C_L (linear interpolation of 30 data), *dashed blue* line = high-fidelity C_L (linear interpolation), *blue* symbols = high-fidelity data, *dotted black* line = piecewise linear interpolation, *black* line = multi-fidelity prediction. Bottom: Interpolation error $\tilde{\epsilon}$.

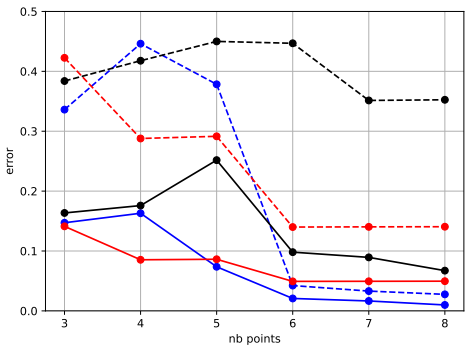

Figure 9: Comparison of error convergence for RANS with two Reynolds numbers. Solid lines = L_2-norm, dotted lines = L_∞-norm. *Blue*: Proposed ANN strategy, *red*: GP-based strategy, *black*: Uniform sampling with ANN.

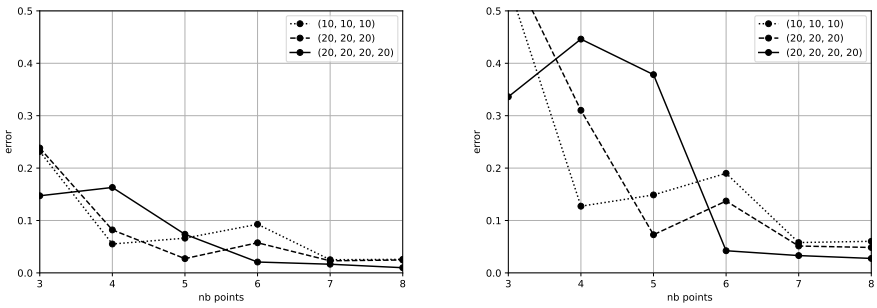

(a) L_2 norm error. (b) L_∞ norm error.

Figure 10: Network size sensitivity for RANS at two Reynolds numbers.

5. References

[1] Pierre Benard, Guillaume Balarac, Vincent Moureau, Cecile Dobrzynski, Ghislain Lartigue, and Yves d'Angelo. Mesh adaptation for large-eddy simulations in complex geometries. *International journal for numerical methods in fluids*, 81(12):719–740, 2016.

[2] Thomas Berthelon, Guillaume Sahut, Julien Leparoux, Guillaume Balarac, Ghislain Lartigue, Manuel Bernard, Vincent Moureau, and Olivier Métais. Toward the use of les for industrial complex geometries. part ii: Reduce the time-to-solution by using a linearised implicit time advancement. *Journal of Turbulence*, 24(6-7):311–329, 2023.

[3] Raghu Bollapragada, Jorge Nocedal, Dheevatsa Mudigere, Hao-Jun Shi, and Ping Tak Peter Tang. A progressive batching l-BFGS method for machine learning. In Jennifer Dy and Andreas Krause, editors, *Proceedings of the 35th International Conference on Machine Learning*, volume 80 of *Proceedings of Machine Learning Research*, pages 620–629. PMLR, 10–15 Jul 2018.

[4] M. Giselle Fernández-Godino. Review of multi-fidelity models. *Advances in Computational Science and Engineering*, 1(4):351–400, 2023.

[5] Alexander IJ Forrester, András Sóbester, and Andy J Keane. Multi-fidelity optimization via surrogate modelling. *Proceedings of the royal society a: mathematical, physical and engineering sciences*, 463(2088):3251–3269, 2007.

[6] Mehdi Ghoreyshi, Keneth Badcock, and Mark Woodgate. Integration of multi-fidelity methods for generating an aerodynamic model for flight simulation. In *46th AIAA aerospace sciences meeting and exhibit*, page 197, 2008.

[7] A Grenouilloux, J Leparoux, V Moureau, G Balarac, T Berthelon, R Mercier, M Bernard, P Bénard, G Lartigue, and O Métais. Toward the use of les for industrial complex geometries. part i: automatic mesh definition. *Journal of Turbulence*, 24(6-7):280–310, 2023.

[8] Zhong-Hua Han, Zimmermann, and Stefan Görtz. Alternative cokriging method for variable-fidelity surrogate modeling. *AIAA journal*, 50(5):1205–1210, 2012.

[9] M. C. Kennedy and A. O'Hagan. Predicting the output from a complex computer code when fast approximations are available. *Biometrika*, 2000.

[10] Matthias Kraushaar. *Application of the compressible and low-Mach number approaches to Large-Eddy Simulation of turbulent flows in aero-engines*. Theses, Institut National Polytechnique de Toulouse - INPT, December 2011.

[11] Loic Le Gratiet and Josselin Garnier. Recursive co-kriging model for design of computer experiments with multiple levels of fidelity. *International Journal for Uncertainty Quantification*, 4(5), 2014.

[12] Oriol Lehmkuhl Barba, Aleix Baez Vidal, Ivette María Rodríguez Pérez, and Carlos David Pérez Segarra. Direct numerical simulation and large-eddy simulations of the turbulent flow around a naca-0012 airfoil. In *7th International conference on computational heat and mass transfer*, pages 1–8, 2011.

[13] Xuhui Meng and George Em Karniadakis. A composite neural network that learns from multi-fidelity data: Application to function approximation and inverse pde problems. *Journal of Computational Physics*, 401:109020, 2020.

[14] Andrew Mole, Alex Skillen, and Alistair Revell. Multi-fidelity surrogate modelling of wall mounted cubes. *Flow, Turbulence and Combustion*, 2023.

[15] Vincent Moureau, Pascale Domingo, and Luc Vervisch. Design of a massively parallel cfd code for complex geometries. *Comptes Rendus Mécanique*, 339(2):141–148, 2011. High Performance Computing.

[16] Franck Nicoud, Hubert Baya Toda, Olivier Cabrit, Sanjeeb Bose, and Jungil Lee. Using singular values to build a subgrid-scale model for large eddy simulations. *Physics of Fluids*, 23(8):085106, 08 2011.

[17] Riccardo Pellegrini, Jeroen Wackers, Riccardo Broglia, Andrea Serani, Michel Visonneau, and Matteo Diez. A multi-fidelity active learning method for global design optimization problems with noisy evaluations. *Engineering with Computers*, 39(5):3183–3206, 2023.

[18] Maziar Raissi and George Karniadakis. Deep multi-fidelity gaussian processes. *arXiv preprint arXiv:1604.07484*, 2016.

[19] Philippe Spalart and Steven Allmaras. A one-equation turbulence model for aerodynamic flows. In *30th aerospace sciences meeting and exhibit*, page 439, 1992.